Electronic Supplementary Information

Rational Design of One-Dimensional Hybrid Organic-Inorganic Perovskites with Room-Temperature Ferroelectricity and Strong Piezoelectricity

Daibei Yang,[ab] Lingheng Luo,[ab] Yi Gao,[c] Shuang Chen*[ad] and Xiao Cheng Zeng*[ef]

[a] Kuang Yaming Honors School, Nanjing University, Nanjing, Jiangsu 210023, China. E-mail: chenshuang@nju.edu.cn

[b] School of Chemistry and Chemical Engineering, Nanjing University, Nanjing, Jiangsu 210023, China.

[c] Division of Interfacial Water and Key Laboratory of Interfacial Physics and Technology, Shanghai Institute of Applied Physics, Chinese Academy of Sciences, Shanghai 201800, China.

[d] Institute for Brain Sciences, Nanjing University, Nanjing 210023, China.

[e] Department of Chemistry, University of Nebraska–Lincoln, Lincoln, Nebraska 68588, United States. E-mail: xzeng1@unl.edu

[f] Beijing Advanced Innovation Center for Soft Matter Science and Engineering, Beijing University of Chemical Technology, Beijing 100029, China.

I. Computational details

All the first-principles calculations of the 1D perovskites are performed by using the Perdew-Burke-Ernzenhof (PBE) exchange-correlation functional within the framework of the generalized gradient approximation (GGA), as implemented in the Vienna ab initio simulation package (VASP) 5.3.5. The Grimme's correction (D3) is also adopted to account for weak van der Waals interactions. The electron-ion interaction is described by the projector augmented wave (PAW) potentials with an energy cut-off of 500 eV. The Gaussian smearing with the width of 0.05 eV is used for the calculations. The structures of three model systems can be taken from the experimental crystallographic data.[S1-S3] For their geometry optimization, the total energy change is set to be less than 10^{-5} eV and the magnitude of the largest force acting on the atoms is set to be less than 0.02 eV/Å. The Brillouin zones are sampled using a 5×2×6 *k*-point mesh for (pyrrolidinium)$MnCl_3$ and (3-pyrrolinium)$MnCl_3$ crystals and a 5×3×8 *k*-point mesh for TMCM-$MnCl_3$ crystal in the Monkhorst–Pack scheme, respectively. To demonstrate the phase-transition mechanism, the climbing-image nudged elastic band (CI-NEB) calculations[S4] are performed to seek possible reaction pathway that connects the initial ferroelectric phase (FP) to the final symmetry-corresponding ferroelectric phase via the paraelectric phase (PP) as the transition state (TS). For the CI-NEB calculations with lattice relaxation, the total energy change is set to be less than 10^{-5} eV and the magnitude of the largest force acting on the atoms is set to be less than 0.05 eV/Å. Meanwhile, the Berry phase method [S5-S7] are used to calculate the spontaneous polarization of each crystal. For the spontaneous polarization and energy of every crystal structure along the phase transition pathways, the more accurate spin-polarized calculations with the higher self-consistent-field (SCF) convergence set at 10^{-6} eV are performed to account for on-site Coulomb (*U*) and Exchange (*J*) interactions of localized *d* electrons of Mn atoms. The required *U* and *J* parameters, U = 3.80 eV and J = 0.75 eV, are chosen following a previous study by using the LDA+*U* method.[S8] We note that another recent first-principles investigation of magnetism in metal−organic frameworks

Mn-MOF-74 has shown that the obtained magnetic and electronic properties were consistent with each other when U was changed in the range of 2−8 eV.[S9] In addition, we also examined the effect of different parameters U and J on the electronic and magnetic properties of (3-pyrrolinium)$MnCl_3$ crystal as an example (see Fig. S1). The GGA+U method chosen here predicts nearly the same band structures (Fig. S1a) as the previous work. [S2] We also found that when U and J parameters are changed within 80% and 120 %, both energy barriers and polarizations are little affected (Fig. S1b and c).

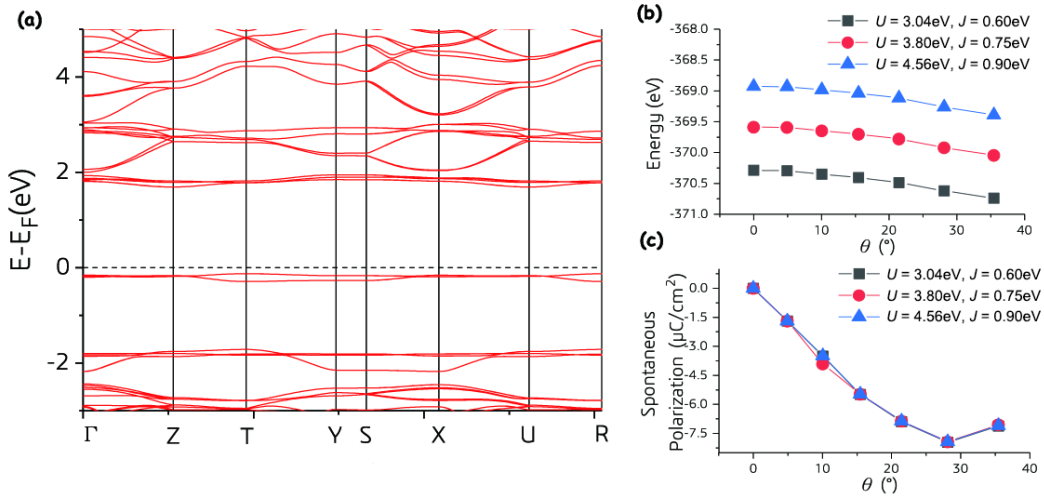

Figure S1. Choice of on-site Coulomb (U) and Exchange (J) interaction parameters: (a) band structures of (3-pyrrolinium)$MnCl_3$ crystal (low-temperature state) by using U = 3.80 eV and J = 0.75 eV, and variations of (b) relative energies and (c) polarizations with rotation angle θ defined in Fig. 2 of the main text by using different U and J parameters.

Noticeably, the magnetism of 1D $AMnCl_3$ perovskites only depends on spin configuration of each Mn site. To determine the magnetic ground states of the 1D perovskites, we performed examined magnetic state for three model systems as shown in Fig. S2. For the three $AMnCl_3$ perovskites, their unit cells include four unit formulas. As a result, we can examine five different magnetic states, including one ferromagnetic (FM) state, three antiferromagnetic (AFM-1, AFM-2, and AFM-3)

states, and one ferrimagnetic (FIM) state, for each HOIP system (Fig. S2a). For (pyrrolidinium)$MnCl_3$, (3-pyrrolinium)$MnCl_3$, and TMCM-$MnCl_3$, their magnetic ground states are all antiferromagnetic (two degenerate AFM-1 and AFM-2 states), fully consistent with the previous first-principles calculations of HOIP $(CH_3CH_2NH_3)Mn(HCOO)_3$ in that the predicted the ground magnetic states of this HOIP were antiferromagnetic, even under strain.[S10] Interestingly, we find that the phase transition energy barrier is almost independent of a certain magnetic state for each 1D perovskite, as indicated by similar tendency of energy change even for different magnetic states as each crystal undergoes the phase transition from ferroelectric phase to paraelectric phase (Fig. S2b-d).

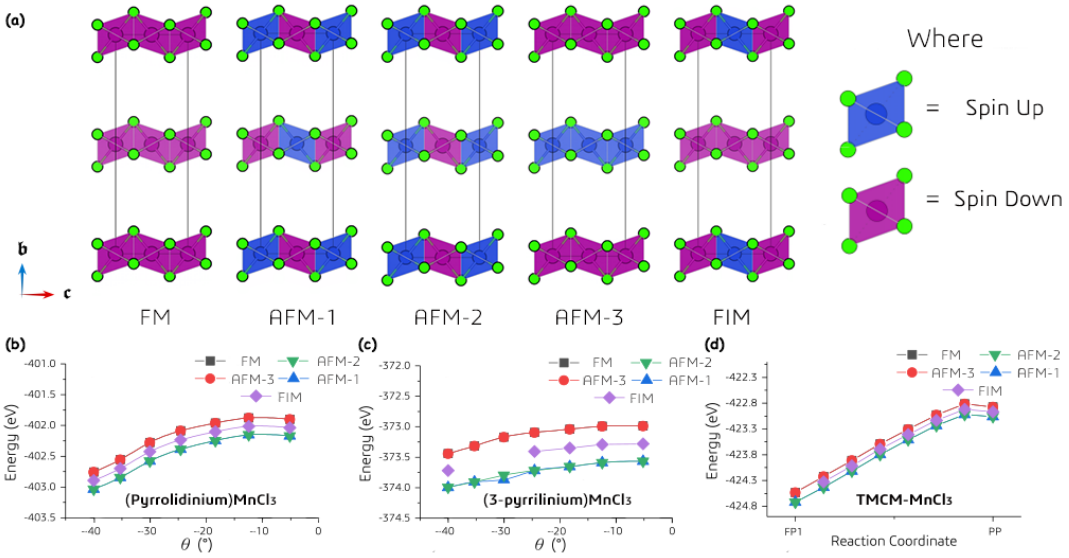

Figure S2. Test of ground magnetic states of one-dimensional (1D) $AMnCl_3$-type hybrid organic-inorganic perovskites (HOIPs): (a) different states expressed by different spin configurations of Mn sites in a unit cell and energy of each state with a specific magnetic state along the phase transition pathway in Fig. 2, 3, and 5 of the main text for (b) (pyrrolidinium)$MnCl_3$, (c) (3-pyrrolinium)$MnCl_3$, and (d) TMCM-$MnCl_3$ crystals respectively. Blue and purple Mn sites in (a) indicate spin up and spin down respectively. The magnetic moment of each Mn site is set as 4.4 μB. For clarity, organic cations have been omitted in each unit cell.

In the following, the mentioned molecular dipole moments of organic cations are all calculated at the level of B3LYP/6-311G(d, p), implemented in the Gaussian 09 program.

II. N-H···Cl hydrogen bonds in the ferroelectric/paraelectric phase of (pyrrolidinium)$MnCl_3$ or (3-pyrrolinium)$MnCl_3$ crystals

Further learned from details of N−H···Cl hydrogen bonds during the phase transition in (pyrrolidinium)$MnCl_3$ or (3-pyrrolinium)$MnCl_3$ in Fig. S3, we found that hydrogen bonds in the ferroelectric phases are formed, with the H_1···Cl_1 (H_1···$Cl_{1'}$) bond length being about 2.3 Å, longer than 2.2 Å. So it can be viewed as weak hydrogen bonds.[S11] In the paraelectric phases of either (pyrrolidinium)$MnCl_3$ or (3-pyrrolinium)$MnCl_3$, H_1 atoms form hydrogen bonds with the other Cl_2 atoms of 1D anionic chains, with the bond length being about 2.6 Å due to the swing-like motion of quasi-planar organic cations. H_1 atoms still form hydrogen bonds with one more Cl_3 atoms with the bond length being about 2.7 Å in (3-pyrrolinium)$MnCl_3$. But the H_1···Cl_3 bond length with a value of about 3.1 Å in (pyrrolidinium)$MnCl_3$ is too long to be viewed as hydrogen bond. Our proposed phase transition mechanism (Fig. 2a of the main text) for (pyrrolidinium)$MnCl_3$ or (3-pyrrolinium)$MnCl_3$, swinging about ring planes of organic cations, is quite different from that based on the experimental XRD analyses.[S2, S3] The previous experiments proposed that the in-plane swing-like motion about the N atom was fixed by the N−H···Cl hydrogen-bonding interactions.[S2, S3] We also examined another possible phase transition pathway of (pyrrolidinium)$MnCl_3$, which is related to a new high-temperature phase proposed by a previous experiment, where the swing center of organic cation is fixed by N atom associated with the N−H_1···Cl_1 hydrogen bond. The resulting energy barrier is as high as about 57.3 kcal/mol, much higher than that (20.2 kcal/mol) calculated based on our proposed mechanism (Fig. 2a of the main text).

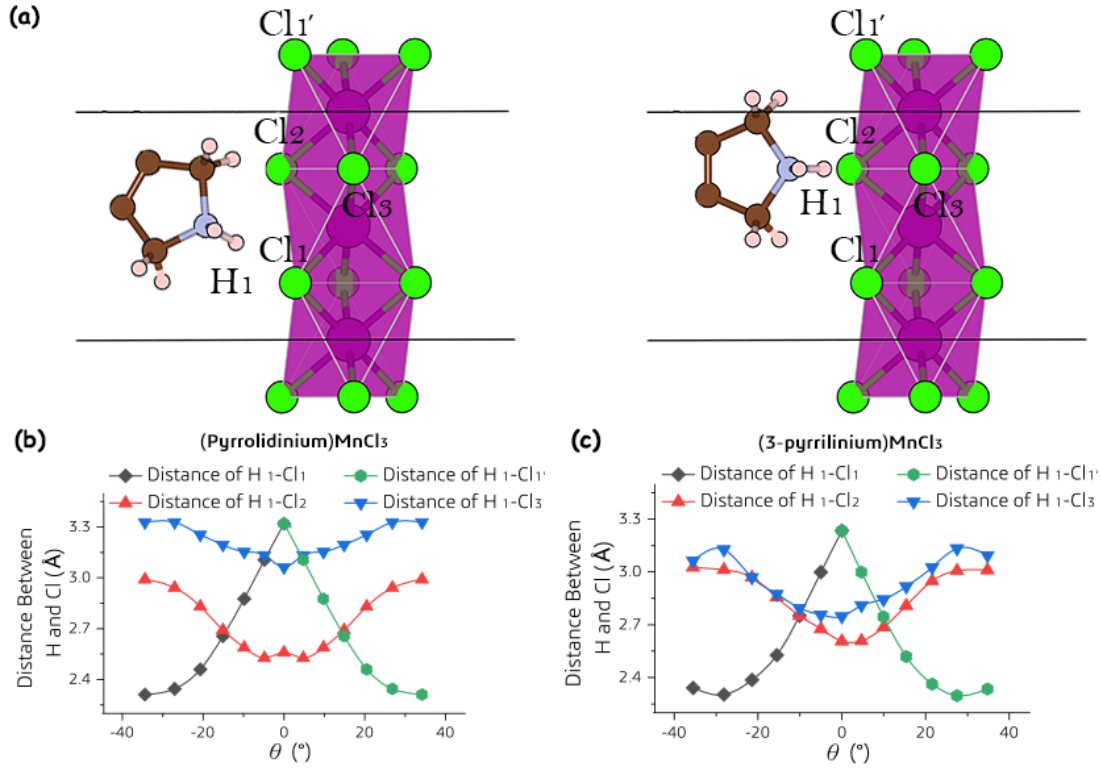

Figure S3. Hydrogen bonding in the (pyrrolidinium)$MnCl_3$ and (3-pyrrolinium)$MnCl_3$ during phase transition: (a) possible hydrogen bonding in ferroelectric phase (Left) and paraelectric phase (Right), highlighted by one formula unit in each $AMnCl_3$ crystal, and variation of different hydrogen bonds with the reaction coordinate (rotation angle, θ) for (b) (prrolidinium)$MnCl_3$ and (c) (3-pyrrolinium)$MnCl_3$, respectively.

Table S1. Summary of structural parameters of inorganic chains in the (3-pyrrolinium)$MnCl_3$ crystal when this crystal undergoes phase transition described by the change of rotation angle (θ) in Fig. 2 of the main text from the ferroelectric phase to the paraelectric phase.

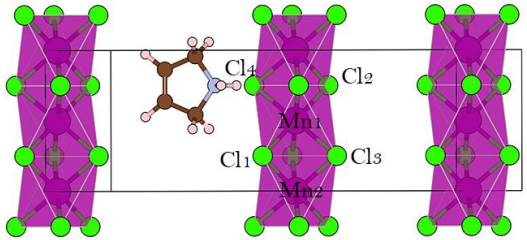

θ	Bond Angle (°)					Bond Length (Å)	
	Cl_1-Mn_1-Cl_2	Cl_1-Mn_1-Cl_3	Cl_1-Mn_1-Cl_4	Mn_1-Mn_2-Cl_1	Mn_1-Mn_2-Cl_2	Cl_1-Mn_1	Cl_1-Mn_2
-35.45	178.71	84.34	94.65	50.65	51.20	2.36	2.33
-28.11	178.97	84.81	94.29	51.01	51.41	2.35	2.33
-21.43	178.75	85.30	93.65	51.40	51.66	2.35	2.33
-15.48	178.87	85.26	93.80	51.43	51.53	2.35	2.33
-10.04	179.08	85.04	94.19	51.35	51.28	2.35	2.32
-4.94	179.51	84.79	94.79	51.26	50.99	2.35	2.33
0	179.97	84.61	95.39	51.23	50.71	2.35	2.33

Table S2. Three investigated and newly designed 1D $AMnCl_3$-type HOIPs in this study with the spontaneous polarization (P_s), change of lattice parameter β, and phase transition energy barriers, based on the first-principles calculations.

A	Chemical Formula for A	B	X	P_s ($\mu C/cm^2$)	β Change (º)	Energy Barrier (kcal/mol)
Model Systems						
Pyrrolidinium	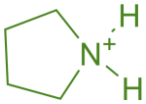	Mn	Cl	7.7 (average)	/	20.2
3-pyrrolinium	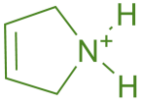	Mn	Cl	7.9	/	10.4
Chloromethyl-trimethyl-ammonium	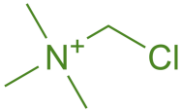	Mn	Cl	8.0	4.0	40.0
Newly Designed 1D Perovskites						
Fluoromethyl-trimethyl-ammonium	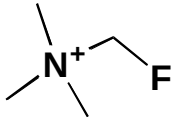	**Mn**	**Cl**	**16.9**	**1.8**	**27.8**
Bromomethyl-trimethyl-ammonium	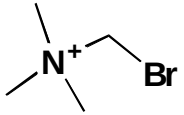	**Mn**	**Cl**	**5.0**	**3.0**	**41.1**

Trimethyl-trimethylsilanyloxymethyl-ammonium		Mn	Cl		Fail in Optimization	
4-(2,2,2-Trifluoro-ethyl)-hexahydro-pyrrolizinium	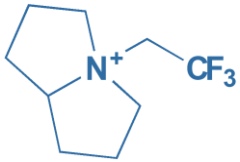	Mn	Cl		Fail in CI-NEB	
1-Methyl-1-(2,2,2-trifluoro-ethyl)-pyrrolidinium	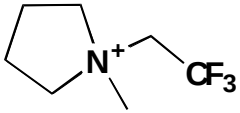	**Mn**	**Cl**	**8.8**	**5.3**	**24.5**
Diethyl-methyl-(2-fluoroethyl)-ammonium	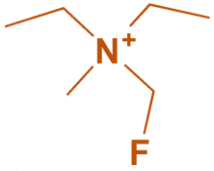	**Mn**	**Cl**	**24.3**	**7.8**	**20.4**
Trimethyl-(2,2,2-trichloro-ethyl)-ammonium	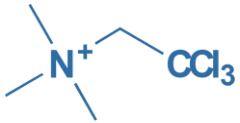	Mn	Cl		Fail in Optimization	
Bromomethyl-tris-trichloromethyl-ammonium	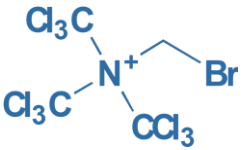	Mn	Cl		Fail in Optimization	
Bromomethyl-bis-chloromethyl-methyl-ammonium	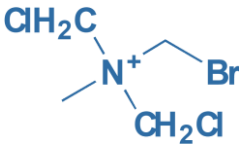	Mn	Cl		Fail in CI-NEB	

Trimethyl-(2,2,2-tribromo-ethyl)-ammonium	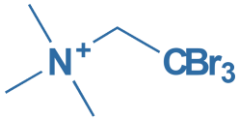	Mn	Cl	/	1.4	> 300
Trimethyl-(2,2,2-trifluoroethyl)-ammonium	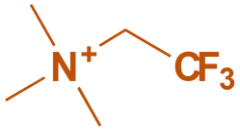	**Mn**	**Cl**	**14.6**	**1.2**	**46.4**
Trimethyl-sulfomethyl-ammonium	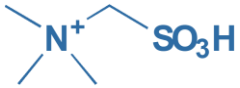	Mn	Cl		Fail in CI-NEB	
Methoxysulfonylmethyl-trimethyl-ammonium	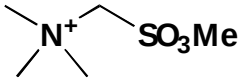	**Mn**	**Cl**	**4.3**	**4.5**	**62.8**
Trimethyl-(2-oxo-ethyl)-ammonium	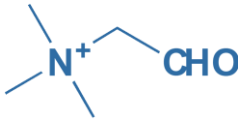	Mn	Cl		Fail in Optimization	
Trimethyl-nitromethyl-ammonium	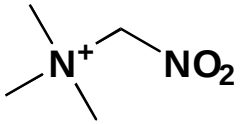	**Mn**	**Cl**	**/**	**10.8**	**35.6**

Table S3. Summary of experimentally reported 1D ABX_3-type HOIPs.

Number	A	B	X	Space Group	
				LTP[a]	HTP[a]
1[S12]	Isopropylammonium	Cd	Br	Pbca	
2[S13]	1,3-thiazol-3-ium	Cd	Br	C2/m	CMCM
3[S14]	Isobutylammonium	Cd	Br	Pnma	CMCM
4[S15-S16]	Tetramethylammonium	Cd	Br	$P6_1$	$P6_3/m$
5[S17]	Trimethyloxosulfonium	Cd	Br	Pnma	
6[S18]	Dimethylammonium	Cd	Cl	$P2_1/c$	$P6_3/m$
7[S13]	1,3-thiazol-3-ium	Cd	Cl	C2/m	CMCM
8[S19]	Tetramethylammonium	Cd	Cl	$P2_1/m$	$P6_3/m$
9[S20]	1,2,4-triazolo-[1,5-a]pyrimidinium	Cd	Cl	$P2_1/c$	
10[S1]	TMCM	Cd	Cl	Cc	$P6_3/mmc$
11[S21]	4-methylpiperidin-1-ium	Cd	Cl	$Pna2_1$	Pnma
12[S22]	Cyclopentanaminium	Cd	Cl	Cc	CMCM
13[S23]	Benzyltrimethylammonium	Cd	Cl	$Pna2_1$	
14[S17]	Trimethyloxosulfonium	Cd	Cl	Pnma	
15[S24]	Pyridinium	Cd	Cl	Pbca	Amma
16[S25]	Trimethylammonium	Cd	Cl	Pcmn	
17[S26]	Pyrrolidinium	Cu	Cl	$P2_1/n$	
18[S27]	Tetramethylammonium	Cu	Cl	$P2_1$	$P6_3/mmc$
19[S28]	Isopropylammonium	Cu	Cl	Pcan	
20[S29]	bis(1,4-Diazoniabicyclo[2.2.2]octane)	K	Cl	R-3c	
21[S30]	Tetramethylammonium	Ni	Br	$P6_3$	
22[S30]	Tetramethylammonium	Ni	Cl	$P6_3$	
23[S31]	N-Methylphenylethylammonium	Ni	Cl	$P2_12_12_1$	
24[S32]	Dimethylammonium	Mn	Cl	$P2_1/c$	$P6_3/m$
25[S2]	3-Pyrrolinium	Mn	Cl	$Cmc2_1$	CMCM
26[S3]	Pyrrolidinium	Mn	Cl	$Cmc2_1$	CMCM
27[S33]	Tetramethylammonium	Mn	Cl	$P2_1/c$	$P6_3/m$
28[S1]	TMCM	Mn	Cl	Cc	$P6_3/mmc$
29[S25]	Trimethylammonium	Mn	Cl	Pcmn	
30[S1]	TMBM	Mn	Br	Cc	$P6_3/mmc$
31[S34]	Pyridinium	Mn	Br	Pbca	
32[S35]	Tetramethylammonium	Sn	I	$P6_3/m$	
33[S36]	(S)-β-phenethylammonium	Pb	Br	$P2_12_12_1$	
34[S37]	N-Butylquinolinium	Pb	Br	$P2_12_12_1$	
35[S38]	benzyl(triethyl)ammonium	Pb	Br	$P2_12_12_1$	
36[S38]	benzyl(triethyl)ammonium	Pb	Cl	$P2_12_12_1$	
37[S39]	1-(Benzylideneamino)pyridinium	Pb	I	$P2_1/c$	
38[S39]	1-(3-Methylbenzylideneamino)pyridinium	Pb	I	$P2_1/c$	
39[S39]	1-(3-Cyanobenzylideneamino)pyridinium	Pb	I	$P6_3$	Not Given

40[S39]	1-(2-Bromobenzylideneamino)pyridinium	Pb	I	$P2_1/c$
41[S39]	1-(2-Chlorobenzylideneamino)pyridinium	Pb	I	$P2_1/c$
42[S39]	1-(4-Bromobenzylideneamino)pyridinium	Pb	I	$P2_1/c$
43[S39]	1-(4-Methylbenzylideneamino)pyridinium	Pb	I	$P2_1/c$
44[S40]	Hexamethylenetetramine	Pb	I	$P2_1/m$
45[S41]	4-cyano-1-n-propylpyridinium	Pb	I	$P2_1/c$
46[S41]	1-benzyl-4-cyanopyridinium	Pb	I	$P2_1/c$

[a]LTP and HTP indicate the low-temperature phase and high-temperature phase of a single crystal, respectively.

III. Estimation of phase transition temperature (T_c)

According to the phase-transition processes (see Figs. 2, 3, and 5) for the five 1D ABX_3 perovskites discussed in the main text, we can use the tenth-degree and sixth-degree polynomial expressions to fit the reaction coordinate (θ)-dependent energy (E) curves, and polarization (P) curves, respectively. Next, the fitting expressions can be plugged into the following equations,

$$\left\langle P^2 \right\rangle = \frac{\int_{\theta_1}^{\theta_2} P^2(\theta) e^{-\beta E(\theta)} \mathrm{d}\theta}{\int_{\theta_1}^{\theta_2} e^{-\beta E(\theta)} \mathrm{d}\theta} \tag{S1}$$

and

$$\chi = \frac{\left\langle P^2 \right\rangle}{3k_B T} \tag{S2}$$

to calculate temperature (T)-dependent polarizability (χ). This method can be found in Ref. S42.

The calculated temperature-dependent polarizability curves are shown in Fig. S4. The inflection point on the polarizability-temperature curve is used to estimate the phase-transition temperatures of 1D perovskites.

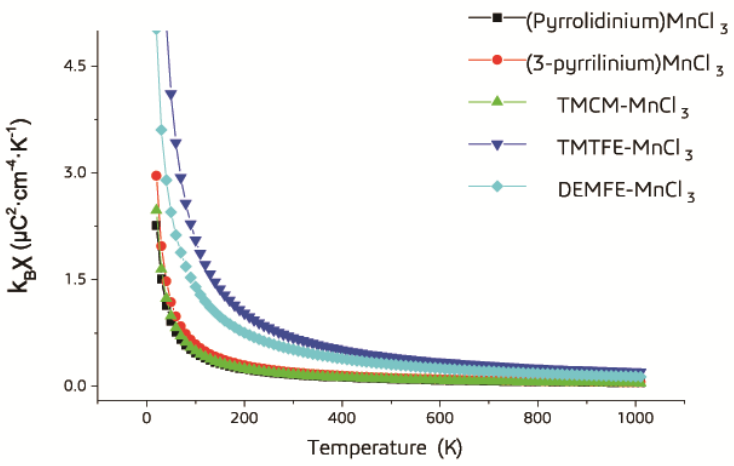

Figure S4. Temperature-dependent polarizability curves for five 1D HOIPs discussed in the main text. Here the vertical coordinate is the product of polarizability (χ) and Boltzmann constant (k_B).

IV. Test of ferroelectric/antiferroelectric states

To confirm the ground state of two newly designed HOIPs, TMTFE-$MnCl_3$ and DEMFE-$MnCl_3$, are ferroelectric rather than antiferroelectric, systems with three different antiferroelectric states were initially built as shown in Fig. S5. Further geometry optimization of these initial systems and subsequent high-accuracy single-point energy computation were carried out. The obtained relative energies with respect to the ferroelectric ground-state energy are summarized in Table S4 to confirm the ferroelectric ground states of both new perovskites.

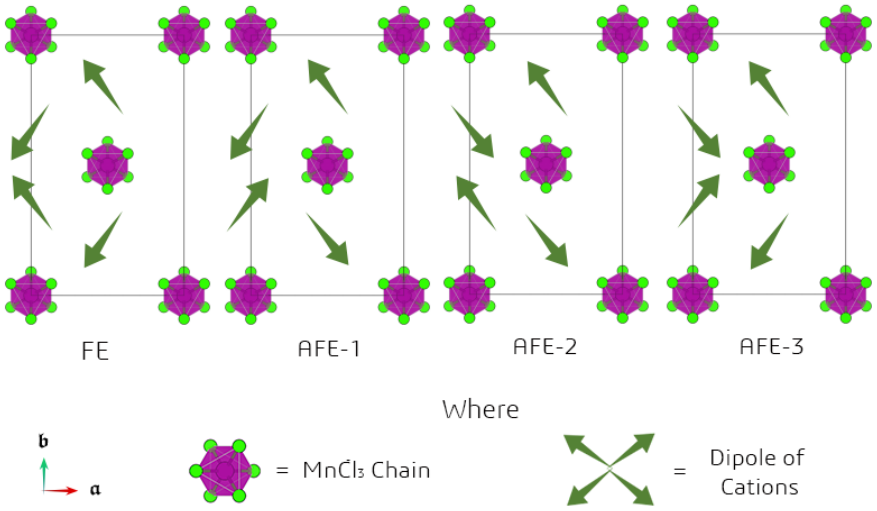

Figure S5. Possible ferroelectric and antiferroelectric states of two newly designed TMTFE-$MnCl_3$ and DEMFE-$MnCl_3$ crystals. Organic cations in each unit cell are omitted and only expressed by their dipole moments (deep green arrows). Purple balls with six light green pearls indicated $MnCl_3$ anions.

Table S4. Summary of relative energies (unit: kcal/mol) of various antiferroelectric states of two newly designed $AMnCl_3$ crystals compared to ferroelectric states discussed in the main text.

State	AFE1	AFE2	AFE3
TMTFE-$MnCl_3$	+1.18	+0.72	+1.66
DEMFE-$MnCl_3$	+5.47	+4.84	+10.2

Supplementary References

S1 Y.-M. You, W.-Q. Liao, D. Zhao, H.-Y. Ye, Y. Zhang, Q. Zhou, X. Niu, J. Wang, P.-F. Li, D.-W. Fu, Z. Wang, S. Gao, K. Yang, J.-M. Liu, J. Li, Y. Yan and R.-G. Xiong, *Science*, 2017, **357**, 306.

S2 H. Y. Ye, Q. Zhou, X. Niu, W. Q. Liao, D. W. Fu, Y. Zhang, Y. M. You, J. Wang, Z. N. Chen and Xiong, R. G. *J. Am. Chem. Soc.*, 2015, **137**, 13148.

S3 Y. Zhang, W. Q. Liao, D. W. Fu, H. Y. Ye, Z. N. Chen and Xiong, R. G. *J. Am. Chem. Soc.*, 2015, **137**, 4928.

S4 H. Jónsson, G. Mills and K. W. Jacobsen, *Nudged Elastic Band Method for Finding Minimum Energy Paths of Transitions*. World Scientific: 1998, p385-404.

S5 R. D. King-Smith and D. Vanderbilt, *Phys. Rev. B*, 1993, **47**, 1651.

S6 D. Vanderbilt and R. D. King-Smith, *Phys. Rev. B*, 1993, **48**, 4442.

S7 R. Resta, *Rev. Mod. Phys.*, 1994, **66**, 899.

S8 I. V. Solovyev, P. H. Dederichs and V. I. Anisimov, *Phys. Rev. B*, 1994, **50**, 16861.

S9 Q. Zhang, B. Li and L. Chen, *Inorg. Chem.*, 2013, **52**, 9356.

S10 S. Ghosh, D. Di Sante and A. Stroppa, *J. Phys. Chem. Lett.*, 2015, **6**, 4553.

S11 T. Steiner, *Angew. Chem. Int. Ed.*, 2002, **41**, 48.

S12 H. Ishihara, K. Horiuchi, S.-q. Dou, M. Gesing Thorsten, J. C. Buhl, H. Paulus, I. Svoboda and H. Fuess, *Zeitschrift für Naturforschung A*, 1999, **54**, 628.

S13 W. Q. Liao, H. Y. Ye, Y. Zhang and R. G. Xiong, *Dalton Trans.*, 2015, **44**, 10614.

S14 Z. Wang, Y. Lu, H. P. Chen and J. Z. Ge, J. Z. *Inorg. Chem.*, 2017, **56**, 7058.

S15 K. J. Gesi, *Phys. Soc. Jpn.*, 1990, **59**, 432.

S16 T. Asahi, K. Hasebe and K. Gesi, *Acta Crystallogr. Sect. C*, 1991, **47**, 1208.

S17 R. Puget, M. Jannin, C. de Brauer and R. Perret, *Acta Crystallogr. Sect. C*, 1991, **47**, 1803.

S18 M. S. Lassoued, W. B. Soltan, M. S. M. Abdelbaky, S. Ammar, A. Gadri, A. B. Salah and S. García-Granda, *J. Mater. Sci.: Mater. Electron.*, 2017, **28**, 12698.

S19 B. Morosin, *Acta Crystallogr. Sect. B*, 1972, **28**, 2303.

S20 C. R. Maldonado, M. Quirós and J. M. Salas, *J. Mol. Struct.*, 2008, **882**, 30.

S21 Y. Lu, Z. Wang, H.-P. Chen and J.-Z. Ge, *CrystEngComm*, 2017, **19**, 1896.

S22 Y. Zhang, H.-Y. Ye, W. Zhang and R.-G. Xiong, *Inorg. Chem. Front.*, 2014, **1**, 118.

S23 D. H. Wu and L. Jin, *Acta crystallogr. Sect C*, 2013, **69**, 491.

S24 X.-F. Sun, Z. Wang, P.-F. Li, W.-Q. Liao, H.-Y. Ye and Y. Zhang, *Inorg. Chem.*, 2017, **56**, 3506.

S25 M. Ravindran, G. R. Willey and M. G. B. Drew, *Inorganica Chimica Acta*, 1990, **175**, 99.

S26 D. M. Nilsen, R. D. Larsen, K. Emerson, G. V. Rubenacker, Z. Ping and J. E. Drumheller, *Inorg. Chem.*, 1990, **29**, 2887.

S27 R. D. Willett, M. R. Bond, W. G. Haije, O. P. M. Soonieus and W. J. A. Maaskant, *Inorg. Chem.*, 1988, **27**, 614.

S28 S. A. Roberts, D. R. Bloomquist, R. D. Willett and H. W. Dodgen, *J. Am. Chem. Soc.*, 1981, **103**, 2603.

S29 F. Thétiot, I. Sasaki, C. Duhayon and J.-P. Sutter, *J. Chem. Crystallogr.*, 2009, **39**, 225.

S30 G. Stucky, *Acta Crystallogr. Sect. B*, 1968, **24**, 330.

S31 R. L. Harlow and S. H. Simonsen, *Acta Crystallogr. Sect. B*, 1977, **33**, 3234.

S32 R. E. Caputo and R. D. Willett, *Phys. Rev. B*, 1977, **16**, 5129.

S33 S. Tancharakorn, F. P. A. Fabbiani, D. R. Allan, K. V. Kamenev and N. Robertson, *J. Am. Chem. Soc.*, 2006, **128**, 9205.

S34 X. Bai, H. Zhong, B. Chen, C. Chen, J. Han, R. Zeng and B. Zou, *J. Phys. Chem. C*, 2018, **122**, 3130.

S35 C. Lode and H. Krautscheid, *Zeitschrift für anorganische und allgemeine Chemie*, 2001, **627**, 841.

S36 D. G. Billing and A. Lemmerer, *Acta Crystallogr. Sect. E*, 2003, **59**, m381.

S37 H.-H. Li, Z.-R. Chen, L.-Q. Guo, K.-N. Ding, J.-Q. Li, C.-C. Huang and Z.-L. Cai, *Aust. J. Chem.*, 2007, **60**, 595.

S38 Y. Niu, X. Chen, Y. Zhu and S. Li, *Sensor. Actuat. B-Chem.*, 2017, **242**, 632.

S39 H.-B. Duan, H.-R. Zhao, X.-M. Ren, H. Zhou, Z.-F. Tian and W.-Q. Jin, *Dalton Trans.*, 2011, **40**, 1672.

S40 M. Hiroshi, N. Hidetsugu, H. Koichi, H. Goro and N. Miharu, *Chem. Lett.*, 1988, **17**, 1907.

S41 Y. Chen, Z. Yang, C.-X. Guo, C.-Y. Ni, H.-X. Li, Z.-G. Ren and J.-P. Lang, *CrystEngComm*, 2011, **13**, 243.

S42 Y. Cai, S. Luo, Z. Wang, J. Xiong and H. Gu, *J Materiomics*, 2017, **3**, 130.